Check for updates

Immobilization of Ag(0) nanoparticles on quaternary ammonium functionalized polyacrylonitrile fiber as a highly active catalyst for 4-nitrophenol reduction†

Jian Xiao, [ID] Zhiying Wu, Kunlang Li, Zibo Zhao and Chunyan Liu*

Ag(0) nanoparticles were immobilized on various pyridine salt, imidazole salt and quaternary ammonium functionalized polyacrylonitrile fibers (PANFs) to prepare Ag(0)-immobilized fiber catalysts. The catalytic activities of these immobilized catalysts for 4-nitrophenol (4-NP) reduction were detected. Among them, the quaternary ammonium fiber with butyl group immobilized Ag(0) nanoparticle catalyst PAN$_{QA-C4}$F-Ag(0) showed the best catalytic activity, and can effectively catalyze 4-nitrophenol (4-NP) reduction with a high conversation rate of 99.6%. Furthermore, PAN$_{QA-C4}$F-Ag(0) can be easily recovered, and it was reused 20 times with little decrease in catalytic activity and moderate Ag retention (53.5%). Notably, the cationic groups in the functionalized fibers can stabilize Ag(0) nanoparticles through electrostatic interactions and steric effects, and play an important role in phase transfer catalysis. Accordingly, possible mechanisms for the 4-NP reduction catalyzed by PAN$_{QA-C4}$F-Ag(0) were proposed.

1. Introduction

Nitrophenol is usually used as a raw material for the preparation of pesticides and dyes.[1–4] Due to its high toxicity and difficulty in degradation, nitrophenol has become a common organic pollutant in waste water.[5–8] Notably, 4-NP is an important kind of nitrophenol compound. It has carcinogenicity, teratogenicity and embryonic cytotoxicity, which can damage the blood, organs and nervous systems of animals, thereby endangering human health.[9–12] In recent years, 4-NP has been regarded as a hazardous pollutant and toxic waste by the U.S. environmental protection agency, and it also became one of the 68 pollutants that are prioritized for treatment in China.

According to recent research, many methods were used to treat 4-NP sewage, including photocatalytic degradation,[13,14] catalytic oxidation,[15] catalytic reduction,[16,17] biodegradation,[18] *etc.* Among them, researchers discovered that 4-NP can be reduced to less toxic 4-aminophenol (4-AP) through using appropriate reducing agents and nano metal catalysts. Therefore, catalytic reduction treatment of 4-NP has high value in environmental protection.

Compared with various precious metals, silver has the advantages of cheap and easy to obtain. Additionally, the supported Ag(0) catalysts have the advantages of high dispersion of Ag(0) nanoparticles, high catalytic activity and easy recovery. Therefore, supported Ag(0) catalysts are more suitable for catalyzing the reduction reaction of 4-NP. Recently, many different materials including SBA-15,[19] GO,[20] polymers,[21,22] MCM-41,[23,24] magnetic Fe_3O_4,[25,26] SiO_2 (ref. 27 and 28) and MOFs[29,30] have been used as supports for preparation of immobilized silver catalysts. These heterogeneous silver catalysts have many advantages, such as high efficiency and simple post-treatment steps. Therefore, preparation of novel heterogeneous Ag(0) nanoparticle catalysts has high research value.

It has been verified that quaternary ammonium salts can effectively stabilize different metal nanoparticles.[31–35] Quaternary ammonium salts also can stabilize Ag(0) nanoparticles through electrostatic interactions and steric effects.[36–40] In this work, various of pyridine salt, imidazole salt and quaternary ammonium functionalized PANFs were prepared by amination and quaternization of PANF. Ag(ı) and Ag(0) nanoparticles were then supported into these pre-functionalized fibers through chelating by –CN in PANF and then reduction. The structures of various functionalized fibers were shown in Scheme 1. The catalytic activities of these Ag(0)-functionalized fibers were tested, and the best fiber catalyst was characterized.

2. Results and discussion

2.1 Preparation and characterization of PANF-immobilized Ag(0) catalysts

Different of PANF-immobilized Ag(0) catalysts have been successfully prepared by chelation of various functionalized

Department of Chemistry, College of Pharmacy, North China University of Science and Technology, Tang Shan, 300072, P. R. China. E-mail: chunyanliu@ncst.edu.cn
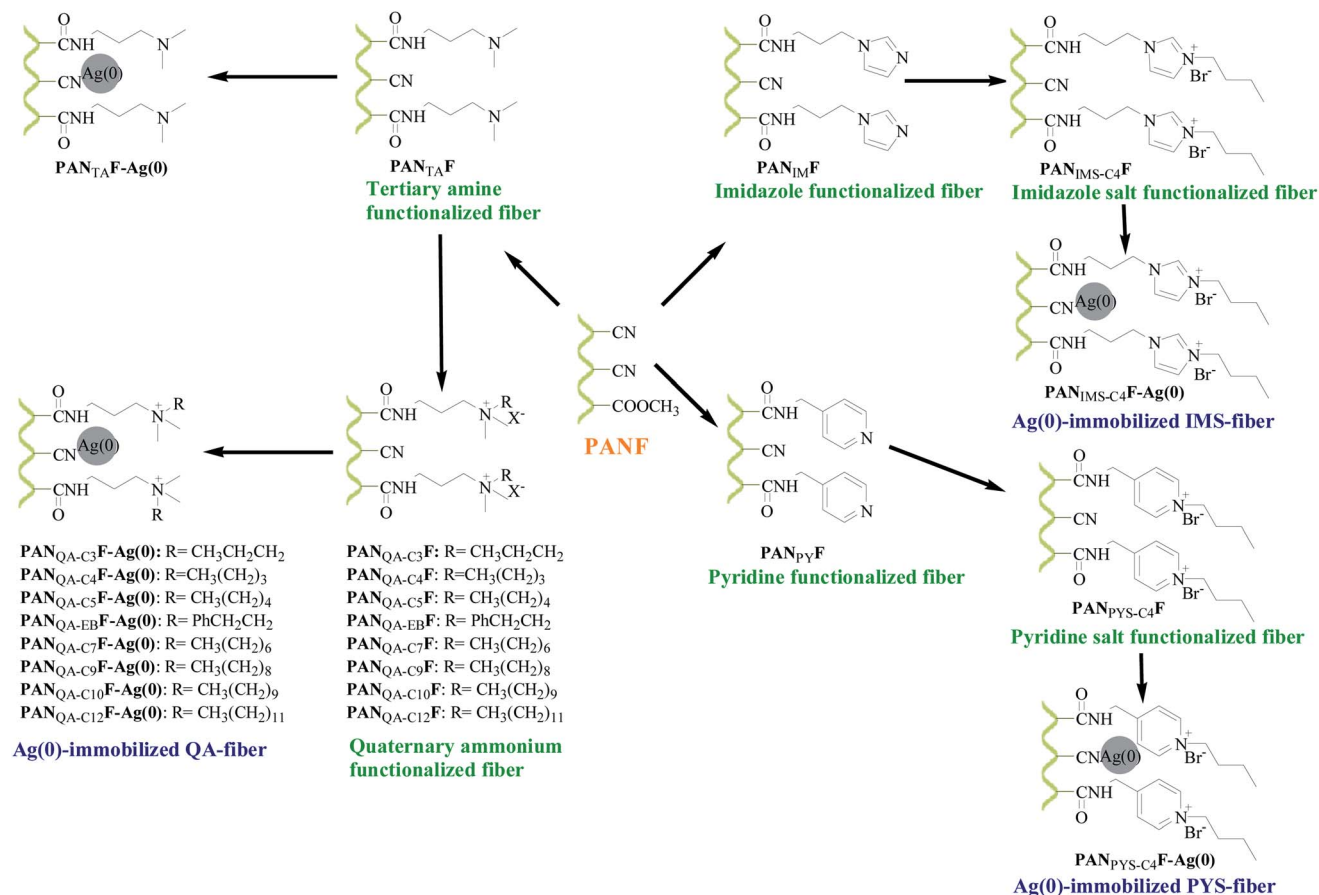
Scheme 1 Various PANF-immobilized silver catalysts[a]. [a] PAN$_{TA}$F is tertiary amine functionalized PANF; PAN$_{PY}$F is pyridine functionalized fiber; PAN$_{IM}$F is imidazole functionalized fiber; PAN$_{PYS}$F is pyridine salt functionalized fiber; PAN$_{IMS}$F is imidazole salt functionalized fiber; PAN$_{QA-C3}$F, PAN$_{QA-C4}$F, PAN$_{QA-C5}$F, PAN$_{QA-EB}$F, PAN$_{QA-C7}$F, PAN$_{QA-C9}$F, PAN$_{QA-C10}$F and PAN$_{QA-C12}$F are ammonium functionalized fibers. PAN$_{TA}$F-Ag(0), PAN$_{IMS}$F-Ag(0), PAN$_{PYS}$F-Ag(0) and PAN$_{QA}$F-Ag(0) are the corresponding fiber-supported Ag(0) nanoparticle catalysts.

PANFs and AgNO$_3$. The functionality of tertiary aminated fiber support was accurately quantified by acid–base titration. The functionalities of PAN$_{IM}$F, PAN$_{PY}$F, PAN$_{QA}$F, PAN$_{IMS}$F and PAN$_{PYS}$F were estimated by $w\%/[M \times (1 + w\%)] \times 1000$, where M is the molecular weight of corresponding moieties and $w\%$ is the weight gain of pre-functionalized PANFs including PANF, PAN$_{TA}$F, PAN$_{IM}$F and PAN$_{PY}$F. Additionally, the functionalities of Ag(0) nanoparticles functionalized PANFs were exactly measured by inductively coupled plasma optical emission spectrometry (ICP-AES). The measured functionality of silver-functionalized PANFs were $5.946–21.700 \times 10^{-3}$ mmol g^{-1}, which verified that Ag(0) nanoparticles were successfully immobilized into surface of fibers. The results of functionality of different fibers are shown in Table 1.

Fourier transform infrared spectroscopy (FTIR) was used to investigate the fiber structures. The FTIR spectra of PANF, PAN$_{TA}$F, PAN$_{QA-C4}$F and PAN$_{QA-C4}$F-Ag(0) are shown in the Fig. 1. The strong adsorption peak at 2243 cm^{-1} was owned to the stretching vibration of C≡N. Compared with PANF, the adsorption peak of C≡N in the functionalized fibers were weakened but did not disappear, showing that the functionalized steps did not damage the skeleton structure of PANF (curve

a). The original fiber has an adsorption peak at 1734 cm^{-1} which is attributed to the stretching vibration of C=O in methoxycarbonyl. After modification, PAN$_{TA}$F has new adsorption peak at 1670 cm^{-1} which is attributed to C=O stretching vibration in carbamoyl, suggesting that the amide was generated by aminolysis of methoxycarbonyl and cyano groups (curves a, b). Each functionalized fiber has an adsorption peak at 3000–3500 cm^{-1}, which is contributed to the stretching vibration of N–H in the amide (curve b–d). Moreover, the FTIR spectrum of PAN$_{QA-C4}$F is similar to that of PAN$_{TA}$F because the quaternary ammonium groups do not have characteristic IR absorption (curve c). Furthermore, compared with PAN$_{QA-C4}$F, the spectrum of PAN$_{QA-C4}$F-Ag(0) did not change significantly, indicating that PAN$_{QA}$F can maintain the integral structure after modification (curve d).

The X-ray diffraction (XRD) was utilized to detect the crystal structure of the fibers and the XRD spectra of PANF, PAN$_{QA-C4}$F-Ag(0) are shown in Fig. 2. Both original fiber and functional fiber have two strong diffraction peaks at 17.0° and 29.5°, which are attributed to the (1 0 0) and (1 1 0) crystallographic planes of hexagonal lattice of PANF (curve a–c). Moreover, the weak peak at $2\theta = 38.1°$ are attributed to (1 1 1) facets of Ag(0) nanoparticle,

Table 1 The functionalities of the various functionalized fibers

Entry	Functionalized fibers	Amount of functionality (mmol g^{-1})	Entry	Functionalized fibers	Amount of functionality (10^{-3} mmol g^{-1})
1	PAN$_{TA}$F	1.985	14	PAN$_{TA}$F-Ag(0)	6.296
2	PAN$_{IM}$F	1.010	15	PAN$_{QA-C3}$F-Ag(0)	7.222
3	PAN$_{PY}$F	1.214	16	PAN$_{QA-C4}$F-Ag(0)	5.946
4	PAN$_{QA-C3}$F	1.883	17	PAN$_{QA-C4}$F-Ag(0)	17.892
5	PAN$_{QA-C4}$F	1.757	18	PAN$_{QA-C4}$F-Ag(0)	28.775
6	PAN$_{QA-C5}$F	1.432	19	PAN$_{QA-C5}$F-Ag(0)	8.610
7	PAN$_{QA-EB}$F	1.523	20	PAN$_{QA-EB}$F-Ag(0)	12.010
8	PAN$_{QA-C7}$F	1.664	21	PAN$_{QA-C7}$F-Ag(0)	9.260
9	PAN$_{QA-C9}$F	1.304	22	PAN$_{QA-C9}$F-Ag(0)	8.980
10	PAN$_{QA-C10}$F	1.288	23	PAN$_{QA-C10}$F-Ag(0)	13.89
11	PAN$_{QA-C12}$F	1.310	24	PAN$_{QA-C12}$F-Ag(0)	21.700
12	PAN$_{IM-C4}$F	0.869	25	PAN$_{IM-C4}$F-Ag(0)	9.800
13	PAN$_{PY-C4}$F	1.064	26	PAN$_{PY-C4}$F-Ag(0)	13.900
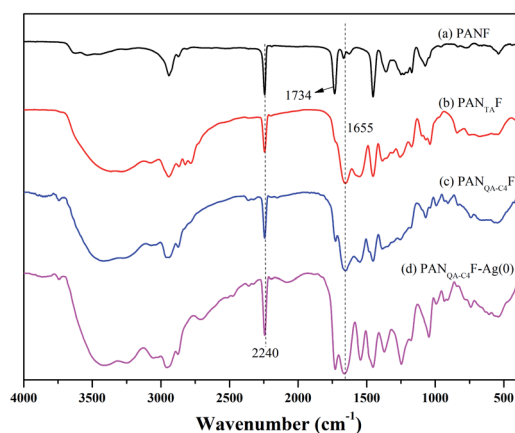
Fig. 1 The FTIR spectra of (a) PANF, (b) PAN$_{TA}$F, (c) PAN$_{QA-C4}$F and (d) PAN$_{QA-C4}$F-Ag(0).
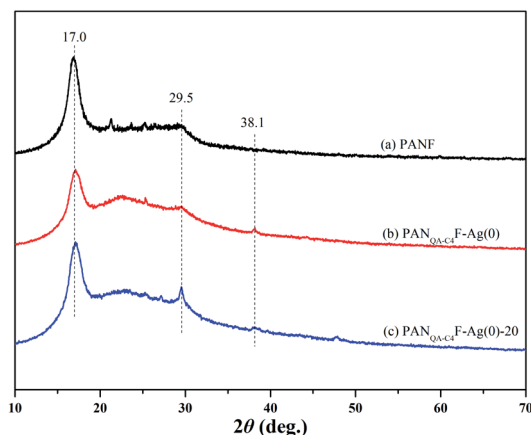
Fig. 2 The XRD spectra of (a) PANF, (b) PAN$_{QA-C4}$F-Ag(0) and (c) PAN$_{QA-C4}$F-Ag(0)-20.

which indicates that the Ag(0) nanoparticle was successfully supported into fiber (curve *b*). Noteworthily, the characteristic diffraction peak of silver still exists in the recycled catalyst,

which proves that the Ag(0) nanoparticles in PAN$_{QA-C4}$F-Ag(0) do not lost seriously after 20th runs (curve *c*).[37]

The elemental analysis (EA) was used to determine the composition of elements of different fibers and the EA data of PANF, PAN$_{TA}$F, PAN$_{QA-C4}$F and PAN$_{QA-C4}$F-Ag(0) are shown in Table 2. Compared with original fiber, PAN$_{TA}$F has less C and N contents and higher H content, the reason is that the immobilized CONHCH$_2$CH$_2$CH$_2$N(CH$_3$)$_2$ moiety has lower C and N contents and more H content (entries 1 and 2). PAN$_{QA-C4}$F has lower C, H, and N contents than PAN$_{TA}$F because of the increased proportion of Br (entry 3). The C, H and N contents of PAN$_{QA-C4}$F-Ag(0) slightly increased because Br$^-$ was partially replaced by NO$_3^-$ (entry 4). EA data proves that fiber has been successfully immobilized.

The X-ray photoelectron spectroscopy (XPS) was applied to detect the chemical properties of the surface of PAN$_{QA-C4}$F-Ag(0), and the result is shown in Fig. 3. The survey spectrum of PAN$_{QA-C4}$F-Ag(0) has obvious peaks of Ag, Br, N, O and C (Fig. 3a). The peaks at 373.4 and 367.4 eV correspond to Ag 3d$_{3/2}$ and Ag 3d$_{5/2}$ of Ag(0), respectively, proving that the Ag(0) nanoparticles have been successfully modified into the fiber (Fig. 3b).[37] Additionally, the corresponding Br 3d spectrum of PAN$_{QA-C4}$F-Ag(0) has a peak at 67.7 eV, which can be attributed to the Br$^-$ in PAN$_{QA-C4}$F-Ag(0) (Fig. 3c). Moreover, there are two peaks at 402.3 and 399.5 eV corresponding to N 1s XPS spectrum of PAN$_{QA-C4}$F-Ag(0), which can be owned to the O=C–N and C–N bonds of the PAN$_{QA-C4}$F-Ag(0), respectively (Fig. 3d). Furthermore, the peak at 529–535 eV was attributed to the O 1s in PAN$_{QA-C4}$F-Ag(0) (Fig. 3e). The peaks at 288.2, 286.4 and

Table 2 The elemental analysis data

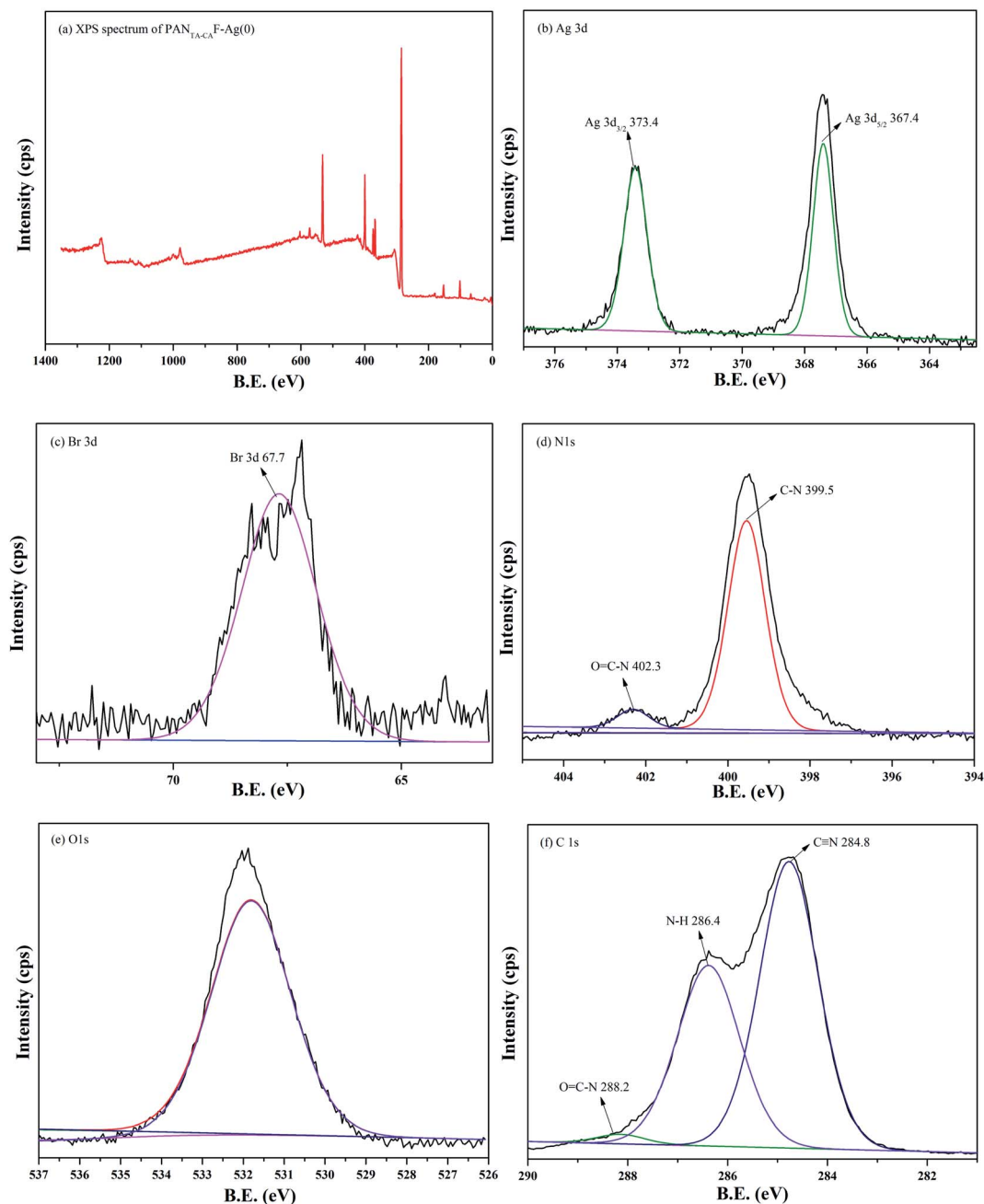| Entry	Fiber	Elemental analysis data		
		C (%)	H (%)	N (%)
1	PANF	66.19	5.98	24.38
2	PAN$_{TA}$F	58.69	7.17	20.65
3	PAN$_{QA-C4}$F	51.42	6.59	15.88
4	PAN$_{QA-C4}$F-Ag(0)	53.90	7.17	16.81

Fig. 3 (a) XPS survey spectrum of $PAN_{QA-C4}F-Ag(0)$, (b) Ag 3d spectra of $PAN_{QA-C4}F-Ag(0)$, (c) Br 3d spectra of $PAN_{QA-C4}F-Ag(0)$, (d) N 1s spectra of $PAN_{QA-C4}F-Ag(0)$, (e) O 1s spectra of $PAN_{QA-C4}F-Ag(0)$ and (f) C 1s spectra of $PAN_{QA-C4}F-Ag(0)$.

284.8 eV corresponding to C 1s XPS spectrum of $PAN_{QA-C4}F-Ag(0)$ owes to the $N-C=O$, $N-H$ and $C\equiv N$ bonds, respectively (Fig. 3f), and the peaks at 980 eV corresponds to C (KLL) Auger electron spectrum (Fig. 3a). XPS spectra further verifies the successfully immobilization of $PAN_{QA-C4}F-Ag(0)$.[41]

Scanning electron microscopy (SEM) images was used to observe the microscopic appearance of the fiber surfaces, so the SEM spectra of various functionalized PANFs are shown in Fig. 4. The functionalized fibers has slightly rough surface under $20\,000\times$ magnification, confirming that its structure was almost not damaged (Fig. 4b–d). Compared with fresh PAN_{QA-}

$_{C4}F-Ag(0)$, the $PAN_{QA-C4}F-Ag(0)$ reused twenty times was not significant broken under $20\,000\times$ magnification, confirming that $PAN_{QA-C4}F-Ag(0)$ can be recycled multiple times because of its good strength (Fig. 4e).

Transmission electron microscopy (TEM) was applied to observe the particle size of the Ag(0) nanoparticles in the $PAN_{QA-C4}F-Ag(0)$. The TEM images of $PAN_{QA-C4}F-Ag(0)$-98 : 1 (the molar ratio of the quaternary ammonium group to the Ag(0) nanoparticle in the catalyst $PAN_{QA-C4}F-Ag(0)$ is 98 : 1) under different magnifications are shown in Fig. 5. The particle size of Ag(0) nanoparticle is about 20–30 nm in fresh $PAN_{QA-C4}F-Ag(0)$, and
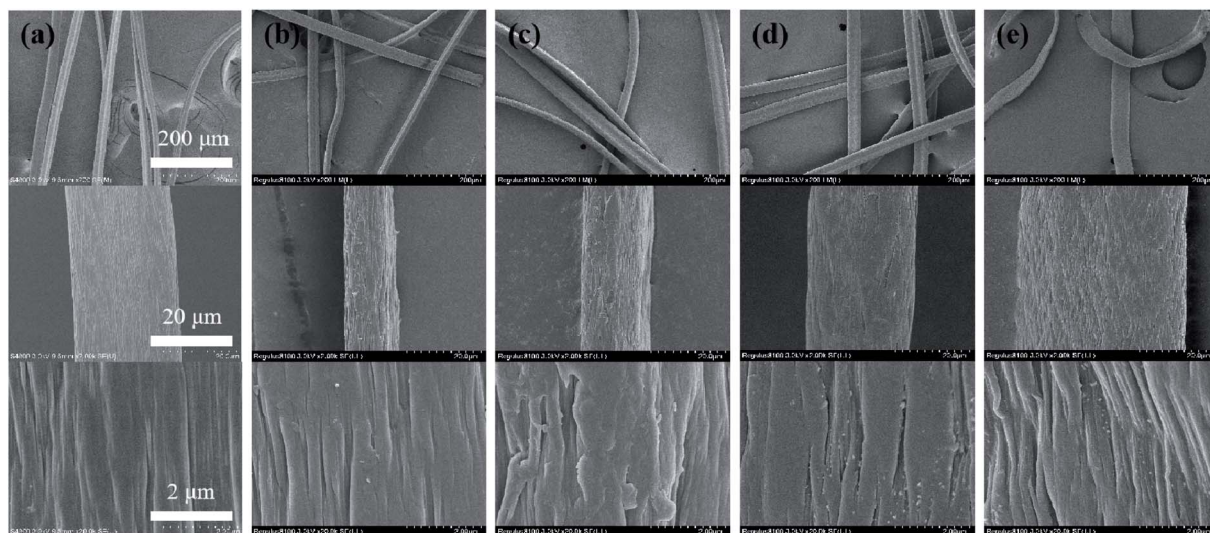
Fig. 4 The SEM images of (a) PANF, (b) $PAN_{TA}F$, (c) $PAN_{QA-C4}F$, (d) $PAN_{QA-C4}F-Ag(0)$ and (e) $PAN_{QA-C4}F-Ag(0)-20$. Top row 200×, middle row 2000× and bottom row 20 000× magnification.

the size of Ag(0) nanoparticles in $PAN_{QA-C12}F-Ag(0)$ is about 10–25 nm, indicating that the fiber catalyst with hydrophobic aliphatic chains is beneficial to stabilize Ag(0) nanoparticles (Fig. S1†). The size of Ag(0) nanoparticles in $PAN_{QA-C4}F-Ag(0)$ used 20 times is still less than 100 nm, suggesting that the nano-sized Ag(0) functionalized fiber catalyst was successfully prepared and has good recyclability.

The thermal stability of PANF, $PAN_{TA}F$, $PAN_{QA-C4}F$ and $PAN_{QA-C4}F-Ag(0)$ were detected by thermogravimetry analysis

(TGA) (Fig. 6). All of the functionalized fibers exhibit lower thermal weight loss and excellent stability under 200 °C, indicating that the fiber catalyst is suitable for general conditions of many reactions (Fig. 6b–d).

2.2 Catalytic activity of PANF-supported Ag catalysts

2.2.1 Catalyst activity of the functionalized fibers.
Various of fiber-supported Ag(0) nanoparticle catalysts were used to catalyze the reduction of 4-NP, and the results are shown in
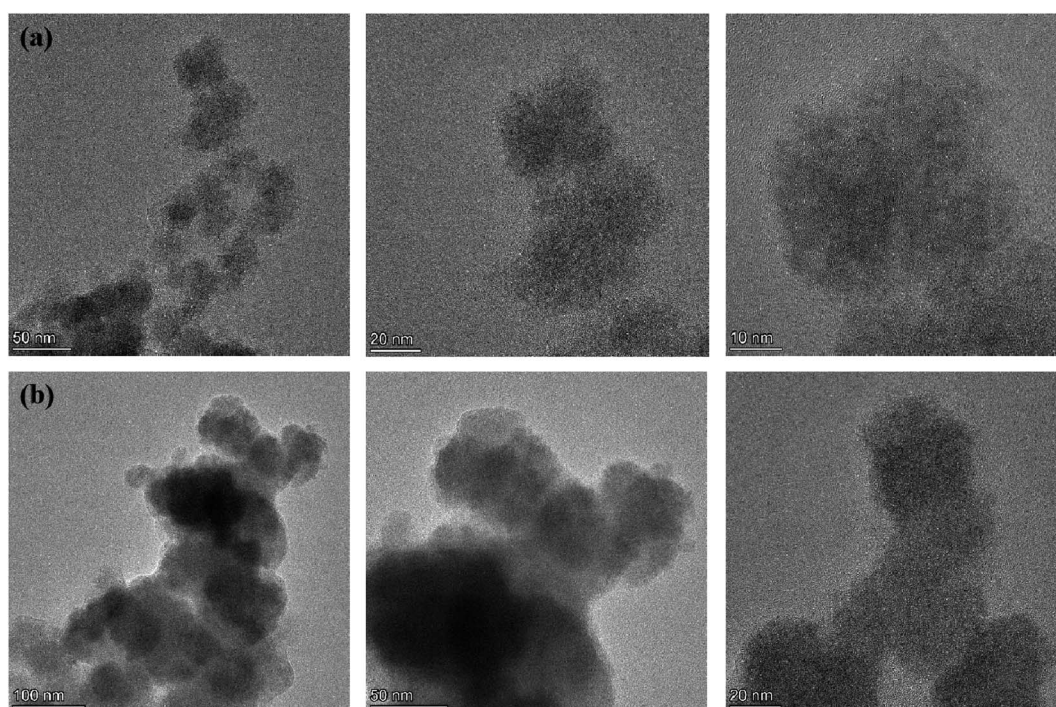

Fig. 5 The TEM images of $PAN_{QA-C4}F-Ag(0)-98:1$, (a) the fresh fiber catalyst and (b) the fiber catalyst used 20 times.
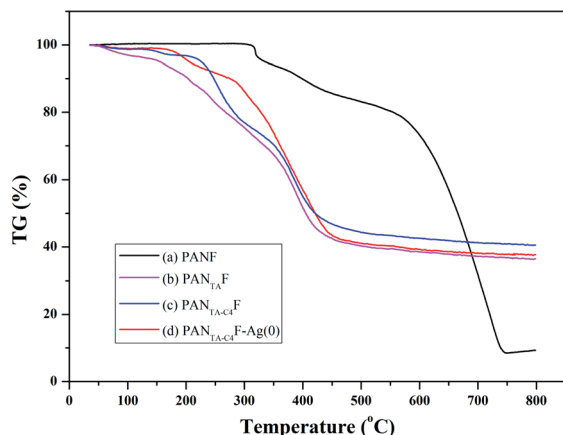
Fig. 6 The thermal stability of (a) PANF, (b) PAN$_{TA}$F, (c) PAN$_{QA-C4}$F and (d) PAN$_{QA-C4}$F-Ag(0).

Table 3. Functionalized fibers with similar quaternary ammonium salt/silver ratios according to close to 300 : 1, 200 : 1, 100 : 1, 60 : 1 are classified into groups one (entries 1–3), group two (entries 4–6), group three (entries 7–12) and group four (entries 13–15), respectively, and the catalytic activities of these fiber catalysts have been detected. The result shows that the quaternary ammonium fiber with butyl group immobilized Ag(0) nanoparticles catalyst PAN$_{QA-C4}$F-Ag(0) showed the best catalytic activity (entries 2, 4, 8 and 13). Compared with PAN$_{TA}$F-Ag(0), PAN$_{QA-C4}$F-Ag(0) has higher catalytic activity, which proves that introduction of quaternary ammonium groups improves the catalytic activity of the fiber catalyst (entries 2, 3, 4,

8 and 13). Through adjusting the ratio of quaternary ammonium salt group and Ag(0) nanoparticle in fiber PAN$_{QA-C4}$F-Ag(0), we found that the fiber PAN$_{QA-C4}$F-Ag(0) has the best catalytic activity when the ratio of quaternary ammonium salt group to silver is close to 100 : 1 (98 : 1) (entry 8). Additionally, different fibers are used to adsorb 4-NP without NaBH$_4$, the result shows that fiber catalysts with short fatty chains have better adsorption effect. The reason can be explainer that 4-NP has good hydrophilicity under alkaline conditions, it is not conducive to the enrichment of 4-NP when the surface layer of the fiber is too hydrophobic (entries 16–22). Above experiments can explain why the PAN$_{QA-C4}$F has the best catalytic activity. Through the above discussion, the catalyst PAN$_{QA-C4}$F-Ag(0)-98 : 1 (the ratio of quaternary ammonium salt to Ag(0) nanoparticle is close to 98 : 1) was selected for subsequent experiments.
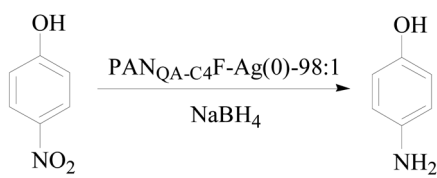
2.2.2 4-NP reduction catalyzed by PAN$_{QA-C4}$F-Ag(0). The conditions of 4-NP reduction reaction catalyzed by PAN$_{QA-C4}$F-Ag(0) were then optimized, and the results are shown in Table 4. Using different amounts of catalyst to catalyze the 4-NP reduction, the optimized removal rate reaches 99.6% when the catalyst loading is 1 mol% and 1.5 mol% (entries 5–7). In addition, the low (50 eq.) or high (200 eq.) dosage of NaBH$_4$ is not conducive to the progress of the reaction, and the best usage of NaBH$_4$ is 100 eq. (entries 3, 5 and 8). The 4-NP conversion rate is low when there is no Ag(0) nanoparticles in the fiber (entry 13). Neither high nor low temperature is not conducive to the reaction, and the best temperature is 25 °C (entries 8–10). Additionally, corresponding control experiments were conducted. The PAN$_{QA-C4}$F-Ag(0) shows adsorption rate of 18.9%

Table 3 The catalytic activities of different fiber catalysts for the reduction of 4-NP[ab]

Entry	Catalyst	The content of Ag(0) (10^{-3} mmol g^{-1})	The content of QA (mmol g^{-1})	The ratio of QA to Ag	Conv. (%)
1	PAN$_{QA-C3}$F-Ag(0)	7.222	1.883	261 : 1	23.4
2	PAN$_{QA-C4}$F-Ag(0)	5.160	1.757	296 : 1	24.9
3	PAN$_{TA}$F-Ag(0)	6.296	1.985	311 : 1	13.5
4	PAN$_{QA-C4}$F-Ag(0)	9.100	1.757	193 : 1	36.5
5	PAN$_{QA-C5}$F-Ag(0)	8.610	1.432	166 : 1	8.5
6	PAN$_{QA-C7}$F-Ag(0)	9.260	1.664	180 : 1	12.3
7	PAN$_{TA}$F-Ag(0)	15.480	1.985	128 : 1	16.2
8	PAN$_{QA-C4}$F-Ag(0)	17.892	1.757	98 : 1	62.1
9	PAN$_{QA-EB}$F-Ag(0)	12.010	1.523	127 : 1	3.5
10	PAN$_{QA-C9}$F-Ag(0)	8.980	1.304	145 : 1	4.6
11	PAN$_{QA-C10}$F-Ag(0)	13.890	1.288	93 : 1	33.2
12	PAN$_{IMS-C4}$F-Ag(0)	9.800	0.869	89 : 1	17.7
13	PAN$_{QA-C4}$F-Ag(0)	28.760	1.757	61 : 1	51.2
14	PAN$_{QA-C12}$F-Ag(0)	21.700	1.310	60 : 1	6.7
15	PAN$_{PY-C4}$F-Ag(0)	13.900	1.064	77 : 1	0.3
16[c]	PAN$_{TA}$F	6.296	1.985	311 : 1	N. R.
17[c]	PAN$_{QA-C3}$F-Ag(0)	7.222	1.883	261 : 1	21.2
18[c]	PAN$_{QA-C4}$F-Ag(0)	9.100	1.757	193 : 1	27.8
19[c]	PAN$_{QA-C5}$F-Ag(0)	8.610	1.432	166 : 1	7.1
20[c]	PAN$_{QA-C7}$F-Ag(0)	9.260	1.664	180 : 1	8.9
21[c]	PAN$_{QA-C10}$F-Ag(0)	13.890	1.288	93 : 1	5.7
22[c]	PAN$_{QA-C12}$F-Ag(0)	21.700	1.310	60 : 1	2.3

[a] General conditions: 0.5 mol% catalyst, 50 eq. NaBH$_4$, 40 mL, 1 mmol L^{-1} 4-NP (aq), and the reaction was carried out in a single neck flask at 25 °C for 6 h. [b] The yields were detected by the standard curve method of UV spectroscopy. [c] General conditions.

Table 4 The catalytic activities of PAN$_{QA-C4}$F-Ag(0) in the different reaction conditions for the reduction of 4-NP

Entry	Catalyst	Catalyst loading	Dosage of NaBH$_4$	Temp. (°C)	Time (min)	Removal rate (%)
1	PAN$_{QA-C4}$F-Ag(0)	0.1 mol%	50 eq.	25	360	3.7
2	PAN$_{QA-C4}$F-Ag(0)	0.5 mol%	50 eq.	25	360	62.1
3	PAN$_{QA-C4}$F-Ag(0)	1 mol%	50 eq.	25	360	97.2
4	PAN$_{QA-C4}$F-Ag(0)	1.5 mol%	50 eq.	25	360	99.1
5	PAN$_{QA-C4}$F-Ag(0)	1 mol%	100 eq.	25	90	99.6
6	PAN$_{QA-C4}$F-Ag(0)	0.5 mol%	100 eq.	25	90	97.7
7	PAN$_{QA-C4}$F-Ag(0)	1.5 mol%	100 eq.	25	45	99.6
8	PAN$_{QA-C4}$F-Ag(0)	1 mol%	200 eq.	25	150	99.6
9	PAN$_{QA-C4}$F-Ag(0)	1 mol%	100 eq.	15	150	97.9
10	PAN$_{QA-C4}$F-Ag(0)	1 mol%	100 eq.	35	110	99.6
11[a]	PAN$_{QA-C4}$F-Ag(0)	1 eq.	—	25	360	27.8
12[a]	PAN$_{QA-C4}$F-Ag(0)	1 eq.	—	35	360	18.9
13	PAN$_{QA-C4}$F	1 eq.	100 eq.	25	600	14.1
14[ab]	PAN$_{QA-C4}$F-Ag(0)	1 eq.	—	25	360	n.r

[a] The pH value of the 4-NP solution is pH = 10. [b] 100 eq. NaBF4 was added in the reaction system.

and 27.8% for 4-NP at 25 °C and 35 °C, which proves that high temperature is not conducive to the accumulation of 4-NP on the surface of the fiber and reduces the catalytic activity of PAN$_{QA-C4}$F-Ag(0) (entries 11 and 12). However, when 100 eq. NaBF$_4$ existed in reaction system, the adsorption capacity of PAN$_{QA-C4}$F-Ag(0) for 4-NP decreased significantly, which indicates that competing anions (BF$_4^-$) in solution can interfere with the enrichment of 4-NP on the fiber(entry 14), and indirectly explains why the catalytic efficiency of PANF decreases when the amount of NaBH$_4$ is too much (entry 8). In summary, the reaction could reach the highest removal rate of 99.6% under the conditions of 1 mol% catalyst loading, 100 eq. NaBH$_4$, 25 °C and 90 min (entry 5).

2.2.3 Reaction kinetic of PAN$_{QA-C4}$F-Ag(0) for 4-NP. The reaction kinetic of 4-NP reduction catalyzed by PAN$_{QA-C4}$F-Ag(0) has been tested. As shown in Fig. 7, the catalysis process conducted slowly within the beginning to 10 min, which can be explained that the 4-NP hardly enrich from the solution to the surface of the fiber within short time. The conversion rate of 4-NP catalyzed by PAN$_{QA-C4}$F-Ag(0) increased rapidly within 10 min to 45 min, and then leveled off after 45 min. The reaction can reach the highest conversion rate of 4-NP (99.6%) at 25 °C. The UV spectra of the 4-NP under different reaction time are shown in Fig. 7b. It can be observed that the absorption peak at 400 nm corresponding to 4-NP decreases significantly as time goes by.

Furthermore, the reaction process can be regarded as a first-order kinetic reaction, and the related equations are shown in eqn (1) and (2).

$$dC_t/dt = -k_{app}t \tag{1}$$

$$\ln(C_t/C_0) = \ln(A_t/A_0) = -k_{app}t \tag{2}$$

where k_{app} is the apparent rate constant (10^{-3} min^{-1}). The plots of $\ln(C_t/C_0)$ vs. time are shown in Fig. 7c, and the k_{app} of the reaction can be calculated to be 55.5 (10^{-3} min^{-1}), suggesting that the PAN$_{QA-C4}$F-Ag(0) has good catalytic activity.

2.2.4 Reusability experiment. Reusability is an important factor in evaluating the performance of heterogeneous catalysts. The reduction of 4-NP was chosen as a model reaction to detect the recycle ability of the catalyst PAN$_{QA-C4}$F-Ag(0). As shown in Fig. 8, after the catalyst was used 20 times, the conversion rate of 4-NP was higher than 99%. As shown in Fig. S3,† the reaction kinetic of 4-NP reduction catalyzed by PAN$_{QA-C4}$F-Ag(0)-20 has been tested, the reaction kinetic curve reaches equilibrium within 90 minutes. The functionality of Ag in PAN$_{QA-C4}$F-Ag(0)-20 detected by ICP-AES is 9.579 $\times$ 10^{-3} mmol g^{-1}, which is moderately lower than that of fresh catalyst PAN$_{QA-C4}$F-Ag(0)-20 (17.892 $\times$ 10^{-3} mmol g^{-1}). The excellent catalytic activity of 4-NP reduction and the moderate Ag-retention (53.5%) shows that the PANF-supported Ag(0) nanocatalyst has moderate stability and reusability.

2.2.5 Ag(0) nanoparticles stabilized by functionalized fiber. Preventing agglomeration of Ag(0) nanoparticles is a main factor in improving fiber-supported Ag(0) catalyst activity. As is mentioned above, the catalytic activity of quaternary ammonium fiber with butyl group immobilized Ag(0) nanoparticles catalyst PAN$_{QA-C4}$F-Ag(0) are better than that of PAN$_{TA}$F-Ag(0), because the steric and electrostatic effects of the quaternary
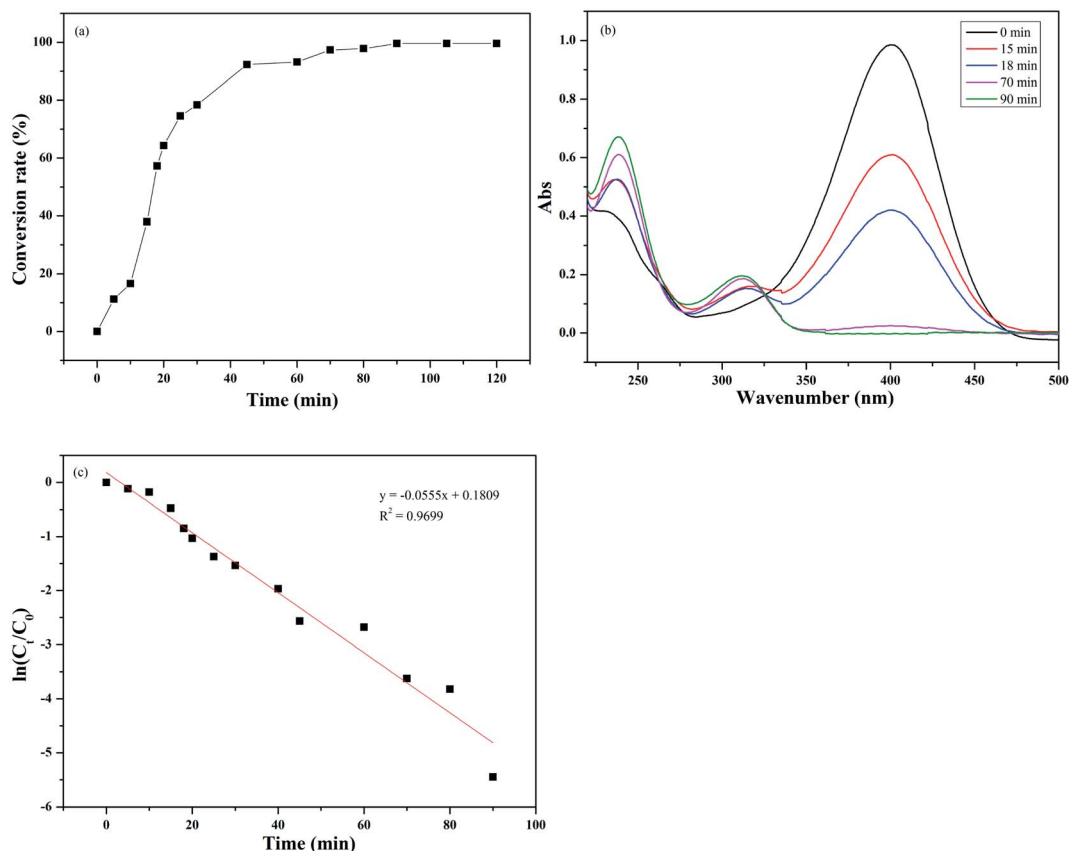
Fig. 7 (a) Catalysis kinetic of $PAN_{QA-C4}F-Ag(0)$ for the reduction of 4-NP at room temperature, (b) UV spectra of reaction system at different times, (c) the plot of $\ln(C_t/C_0)$ vs. time.
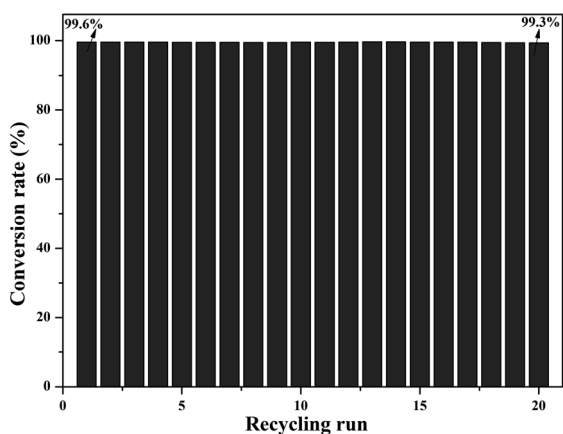

Fig. 8 Reusability experiment of $PAN_{QA-C4}F-Ag(0)-98:1^a$. [a] Reaction conditions: 4-NP (1.00 mmol L^{-1}, 40.0 mL), 1.0 mol% $PAN_{QA-C4}F-Ag(0)-98:1$, 25 °C. The yield was obtained by UV-visible spectrophotometer.

ammonium salts in fibers are more conducive to stabilizing the nanoparticles. As shown in Scheme 2, the halogen ions can stabilize the Ag(0) nanoparticles through chelation, and the butyl chains in the quaternary ammonium salt group can disperse the Ag(0) nanoparticles through steric effect.

2.2.6 The possible mechanisms of fiber-catalyzed 4-NP reduction. The possible mechanisms are proposed and shown in Scheme 3. In the first step, 4-NP can be easily enriched into cationic microenvironment on the surface of the fibers due to the electrostatic attraction. However, the $PAN_{QA-C4}F-Ag(0)$ with low Ag(0) nanoparticle loading and too high quaternary ammonium salt functionality has lower catalytic activity, which
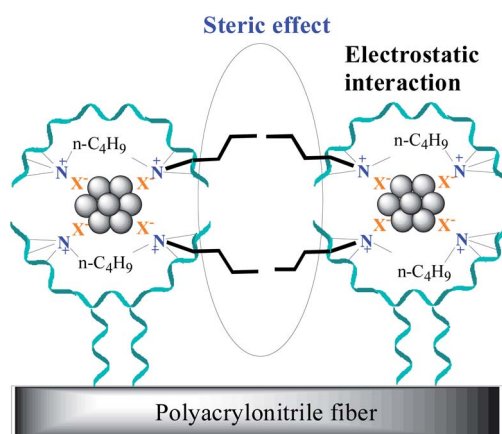
Scheme 2 The stabilization of Ag(0) through steric effect and electrostatic of quaternary ammonium salts functionalized fiber.
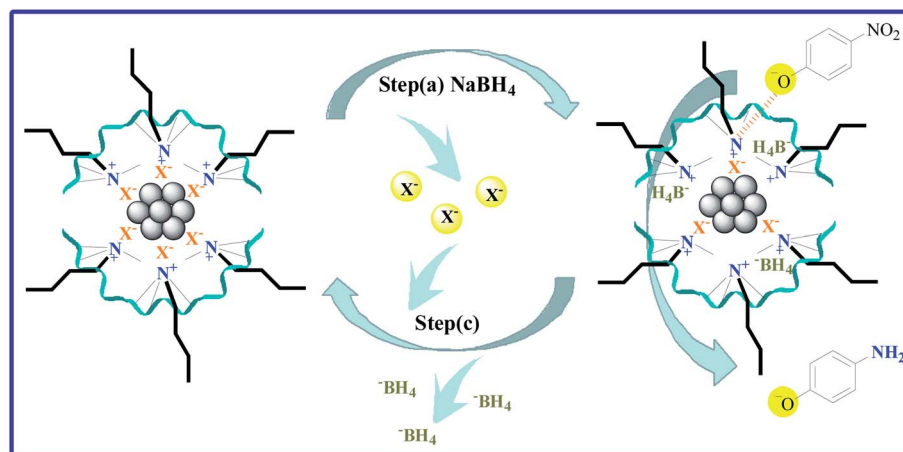
Scheme 3 PAN$_{QA-C4}$F-Ag(0) catalyzed reduction of 4-NP.

can be explained by that the 4-NP is bound to the surface of fiber and cannot move freely, and the low-density silver catalytic sites cannot catalyze the conversion of more reactants. Therefore, compared with the PAN$_{QA-C4}$F-Ag(0)-61 : 1, PAN$_{QA-C4}$F-Ag(0)-193 : 1 and PAN$_{QA-C4}$F-Ag(0)-296 : 1, the PAN$_{QA-C4}$F-Ag(0)-98 : 1 has best catalytic activity. In the second step, 4-aminophenol (4-AP) is reduced to Ag (0) nanoparticles and corresponding anions return to the surface of fiber. The proposal mechanism diagram proves that the cationic microenvironment on the surface of the fiber can promote the reaction.

2.3 Comparison of PAN$_{QA-C4}$F-Ag(0) with other catalytic systems

Compared with other catalysts for 4-NP reduction, fiber-supported Ag(0) nanoparticle catalyst PAN$_{QA-C4}$F-Ag(0) shows moderate performance. The result was shown in Table S1.† The 4-NP reduction catalyzed by PAN$_{QA-C4}$F-Ag(0) has the advantages of high conversion rate and good cycle performance.

Fig. 9 The picture of reaction system before and after reaction. (a) Before reaction, (b) after reaction.

3. Conclusion

Different Ag(0) nanoparticle functionalized fiber catalysts were successfully prepared. Screened by 4-NP reduction, the quaternary ammonium fiber with butyl group immobilized Ag(0) nanoparticles catalyst PAN$_{QA-C4}$F-Ag(0) was chosen as the optimal catalyst for subsequent experiments. PAN$_{QA-C4}$F-Ag(0) can efficiently catalyze the reduction of 4-NP under room temperature with high conversion rate of 99.6%, which proves that PAN$_{QA-C4}$F-Ag(0) has application value in the nitrophenol wastewater treatment. Additionally, possible catalytic mechanisms based on the fiber microenvironment was proposed. Furthermore, the catalytic activity of PAN$_{QA-C4}$F-Ag(0) for the reduction of 4-NP decreased little after 20 times of use, which show its good reusability and practical application potential (Fig. 9).

Conflicts of interest

There are no conflicts to declare.

Acknowledgements

References

1 R. Gao, L. Pan, H. Wang, X. Zhang, L. Wang and J. Zou, Ultradispersed Nickel Phosphide on Phosphorus-Doped Carbon with Tailored d-Band Center for Efficient and Chemoselective Hydrogenation of Nitroarenes, *ACS Catal.*, 2018, **8**, 8420–8429.
2 R. Gao, L. Pan, Z. Li, X. Zhang, L. Wang and J. Zou, Cobalt nanoparticles encapsulated in nitrogen-doped carbon for room-temperature selective hydrogenation of nitroarenes, *Chin. J. Catal.*, 2018, **39**, 664–672.
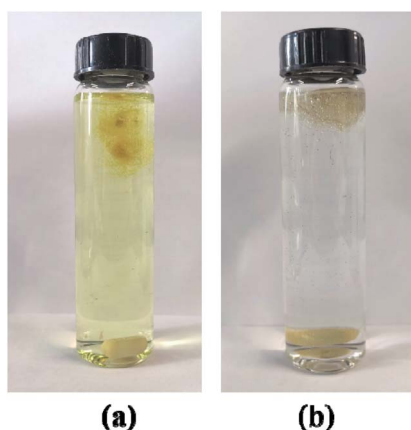
3 M. Yaseen, B. Manu, N. Kudri and H. S. Govardhanaswamy, Use of redox mediators for the enhanced degradation of selected nitrophenols, *Appl. Water Sci.*, 2019, **9**, 194.

4 R. Fatima, M. N. Afridi, V. Kumar, J. Lee, I. Ali, K. Kim and J. Kim, Photocatalytic degradation performance of various types of modified TiO2 against nitrophenols in aqueous systems, *J. Cleaner Prod.*, 2019, **231**, 899–912.

5 X. Liu, L. Zhao, H. Lai, S. Li and Z. Yi, Efficient photocatalytic degradation of 4-nitrophenol over graphene modified TiO2, *J. Chem. Technol. Biotechnol.*, 2017, **92**, 2417–2424.

6 S. Varshney, R. Bar Ziv and T. Zidki, On the Remarkable Performance of Silver-based Alloy Nanoparticles in 4-Nitrophenol Catalytic Reduction, *ChemCatChem*, 2020, **12**, 4680–4688.

7 S. R. Thawarkar, B. Thombare, B. S. Munde and N. D. Khupse, Kinetic investigation for the catalytic reduction of nitrophenol using ionic liquid stabilized gold nanoparticles, *RSC Adv.*, 2018, **8**, 38384–38390.

8 S. Gopi, A. G. Ramu, S. Sakthivel, G. Maia, C. Jang, D. Choi and K. Yun, Cobalt-modified 2D porous organic polymer for highly efficient electrocatalytic removal of toxic urea and nitrophenol, *Chemosphere*, 2021, **265**, 129052.

9 N. Hu, J. Y. Yin and Q. Tang, Comparative study of amphiphilic hyperbranched and linear polymer stabilized organo-soluble gold nanoparticles as efficient recyclable catalysts in the biphasic reduction of 4-nitrophenol, *J. Polym. Sci., Part A: Polym. Chem.*, 2011, **49**, 3826–3834.

10 Y. Liu, Y. Fan and Y. Yuan, Amphiphilic hyperbranched copolymers bearing a hyperbranched core and a dendritic shell as novel stabilizers rendering gold nanoparticles with an unprecedentedly long lifetime in the catalytic reduction of 4-nitrophenol, *J. Mater. Chem.*, 2012, **22**, 21173–21182.

11 N. Hu, J. Y. Yin and Q. Tang, Comparative study of amphiphilic hyperbranched and linear polymer stabilized organo-soluble gold nanoparticles as efficient recyclable catalysts in the biphasic reduction of 4-nitrophenol, *J. Polym. Sci., Part A: Polym. Chem.*, 2011, **49**, 3826–3834.

12 Y. Y. Chu, Y. Qian, W. J. Wang and X. L. Deng, A dual-cathode electro-Fenton oxidation coupled with anodic oxidation system used for 4-nitrophenol degradation, *J. Hazard. Mater.*, 2012, **199–200**, 179–185.

13 K. Chakraborty, S. Chakrabarty, T. Pal and S. Ghosh, Synergistic effect of zinc selenide-reduced graphene oxide towards enhanced solar light-responsive photocurrent generation and photocatalytic 4-nitrophenol degradation, *New J. Chem.*, 2017, **41**, 4662–4671.

14 Q. Yang, E. Guo, H. Liu and Q. Lu, Engineering of Z-scheme 2D/3D architectures with Bi2MoO6 on TiO2 nanosphere for enhanced photocatalytic 4-nitrophenol degradation, *J. Taiwan Inst. Chem. Eng.*, 2019, **105**, 65–74.

15 N. L. McCombs, J. D Antonio, D. A. Barrios, L. M. Carey and R. A. Ghiladi, Nonmicrobial Nitrophenol Degradation *via* Peroxygenase Activity of Dehaloperoxidase-Hemoglobin fromAmphitrite ornata, *Biochemistry*, 2016, **55**, 2465–2478.

16 J. Rong, H. Chen, F. Qiu, T. Zhang, Y. Zhu, D. Yang, J. Xu, X. Rong, Q. Guo and X. Peng, In-situ immobilization and pyrolysis of metal-organic framework supported on

biomorphic layered double hydroxides as highly active and stable heterogeneous catalyst, *J. Taiwan Inst. Chem. Eng.*, 2018, **88**, 78–88.

17 S. Lu, J. Yu, Y. Cheng, Q. Wang, A. Barras, W. Xu, S. Szunerits, D. Cornu and R. Boukherroub, Preparation of silver nanoparticles/polydopamine functionalized polyacrylonitrile fiber paper and its catalytic activity for the reduction 4-nitrophenol, *Appl. Surf. Sci.*, 2017, **411**, 163–169.

18 J. Wang, Y. Li, H. Li, Z. Cui, Y. Hou, W. Shi, K. Jiang, L. Qu and Y. Zhang, A novel synthesis of oleophylic Fe2O3/polystyrene fibers by γ-Ray irradiation for the enhanced photocatalysis of 4-chlorophenol and 4-nitrophenol degradation, *J. Hazard. Mater.*, 2019, **379**, 120806.

19 G. Qiao, Q. Xu, A. Wang, D. Zhou and J. Z. Yin, Efficient synthesis of sub-5 nm Ag nanoparticles by the desorption effect of supercritical CO2 in SBA-15, *Nanotechnology*, 2020, **31**, 375603.

20 Z. Wang, F. Li, L. Zhang, J. Z. Qian and S. K. Cao, Phase-transfer-assisted synthesis of cysteine-Ag nanoparticles/graphene oxide nanocomposite and its enhanced performance in antibiosis and biosensing, *Nanotechnology*, 2020, **31**, 455603.

21 S. Chen, G. Wang, W. Sui, A. M. Parvezc and C. L. Si, Synthesis of lignin-functionalized phenolic nanosphere supported Ag nanoparticles with excellent dispersion stability and catalytic performance, *Green Chem.*, 2020, **22**, 2879–2888.

22 C. Xie, J. Song, H. Wu, Y. Hu, H. Z. Liu, Y. D. Yang, Z. R. Zhang, B. F. Chen and B. X. Han, Naturally occurring gallic acid derived multifunctional porous polymers for highly efficient CO2 conversion and I2 capture, *Green Chem.*, 2018, **20**, 4655–4661.

23 R. V. Sales, H. O. M. A. Moura, A. B. F. Câmara, E. Rodríguez-Castellón, J. A. B. Silva, S. B. C. Pergher, L. M. A. Campos, M. M. Urbina, T. C. Bicudo and L. S. de Carvalho, Assessment of Ag Nanoparticles Interaction over Low-Cost Mesoporous Silica in Deep Desulfurization of Diesel, *Catalysts*, 2019, **9**, 651.

24 Z. Chen and R. L. Luck, Oxidation of olefins using atmospheric oxygen atoms initiated by tert-butylhydroperoxide or hydrogen peroxide with silver nanoparticles deposited on MCM-41 as catalysts, *Green Chem.*, 2016, **18**, 3354–3359.

25 X. Zhang, B. Ren, X. Li, Y. Xu, B. Liu, P. Yu, Y. Sun and D. Mei, Efficiently enhanced visible-light photocatalytic activity by *in situ* deposition of Ag@AgBr on g-C3N4/Fe3O4 magnetic heterogeneous materials, *Sep. Purif. Technol.*, 2021, **254**, 117596.

26 S. Chang, C. Liu, Y. Sun, Z. Yan, X. Zhang, X. Hu and H. Zhang, Fe3O4 Nanoparticles Coated with Ag-Nanoparticle-Embedded Metal-Organic Framework MIL-100(Fe) for the Catalytic Reduction of 4-Nitrophenol, *ACS Appl. Nano Mater.*, 2020, **3**, 2302–2309.

27 J. Huang, X. Han, X. Zhao and C. Meng, Facile preparation of core-shell Ag@SiO2 nanoparticles and their application in spectrally splitting PV/T systems, *Energy*, 2021, **215**, 119111.

28 H. Li, W. Xu, L. Qiu, Y. Wang, L. Xiao, F. Ouyang, L. Lin and X. Chen, Effect of Silver Doping on F-TiO2/SiO2 Nano-Powder Catalysts for Photocatalytic Degradation of Acrylonitrile Wastewater, *J. Nanoelectron. Optoelectron.*, 2019, **14**, 1043–1047.

29 Y. Yang, X. Wu, C. He, J. Huang, S. Yin, M. Zhou, L. Ma, W. Zhao, L. Qiu, C. Cheng and C. Zhao, Metal-Organic Framework/Ag-Based Hybrid Nanoagents for Rapid and Synergistic Bacterial Eradication, *ACS Appl. Mater. Interfaces*, 2020, **12**, 13698–13708.

30 J. Shi, L. Zhang, N. Sun, D. Hu, Q. Shen, F. Mao, Q. Gao and W. Wei, Facile and Rapid Preparation of Ag@ZIF-8 for Carboxylation of Terminal Alkynes with CO2 in Mild Conditions, *ACS Appl. Mater. Interfaces*, 2019, **11**, 28858–28867.

31 F. Xu, Q. Zhang and Z. Gao, Simple one-step synthesis of gold nanoparticles with controlled size using cationic Gemini surfactants as ligands: Effect of the variations in concentrations and tail lengths, *Colloids Surf., A*, 2013, **417**, 201–210.

32 Y. Xu, Y. Zhao, L. Chen, X. Wang, J. Sun, H. Wu, F. Bao, J. Fan and Q. Zhang, Large-scale, low-cost synthesis of monodispersed gold nanorods using a gemini surfactant, *Nanoscale*, 2015, **7**, 6790–6797.

33 D. Li, W. Fang, Y. Feng, Q. Geng and M. Song, Stability properties of water-based gold and silver nanofluids stabilized by cationic gemini surfactants, *J. Taiwan Inst. Chem. Eng.*, 2019, **97**, 458–465.

34 D. Astruc, F. Lu and J. R. Aranzaes, Nanoparticles as Recyclable Catalysts: The Frontier between Homogeneous

and Heterogeneous Catalysis, *Angew. Chem., Int. Ed.*, 2005, **44**, 7852–7872.

35 T. Jain, A. R. Tehrani-Bagha, H. Shekhar, R. Crawford, E. Johnson, K. Nørgaard, K. Holmberg, P. Erhart and K. Moth-Poulsen, Anisotropic growth of gold nanoparticles using cationic gemini surfactants: effects of structure variations in head and tail groups, *J. Mater. Chem. C*, 2014, **2**, 994–1003.

36 S. He, H. Chen, Z. Guo, B. Wang, C. Tang and Y. Feng, High-concentration silver colloid stabilized by a cationic gemini surfactant, *Colloids Surf., A*, 2013, **429**, 98–105.

37 J. Xu, X. Han, H. Liu and Y. Hu, Synthesis and optical properties of silver nanoparticles stabilized by gemini surfactant, *Colloids Surf., A*, 2006, **273**, 179–183.

38 S. Bhattacharya and J. Biswas, Role of spacer lengths of gemini surfactants in the synthesis of silver nanorods in micellar media, *Nanoscale*, 2011, **3**, 2924.

39 S. Datta, J. Biswas and S. Bhattacharya, How does spacer length of imidazolium gemini surfactants control the fabrication of 2D-Langmuir films of silver-nanoparticles at the air-water interface?, *J. Colloid Interface Sci.*, 2014, **430**, 85–92.

40 D. Li, W. Fang, Y. Zhang, X. Wang, M. Guo and X. Qin, Stability and Thermal Conductivity Enhancement of Silver Nanofluids with Gemini Surfactants, *Ind. Eng. Chem. Res.*, 2017, **56**, 12369–12375.

41 G. Xu, J. Cao, Y. Zhao, L. S. Zheng, M. L. Tao and W. Q. Zhang, Phosphorylated Polyacrylonitrile Fiber as an Efficient and Greener Acetalization Catalyst, *Chem.–Asian J.*, 2017, **12**, 2565–2575.